Computational Mechanics
https://doi.org/10.1007/s00466-024-02462-8

ORIGINAL PAPER

Proper generalized decomposition-based iterative enrichment process combined with shooting method for steady-state forced response analysis of nonlinear dynamical systems

Dae-Guen Lim[1] · **Gil-Yong Lee**[2] · **Yong-Hwa Park**[1]

Received: 26 September 2023 / Accepted: 11 February 2024

Abstract
This paper presents a novel framework combining proper generalized decomposition (PGD) with the shooting method to determine the steady-state response of nonlinear dynamical systems upon a general periodic input. The proposed PGD approximates the response as a low-rank separated representation of the spatial and temporal dimensions. The Galerkin projection is employed to formulate the subproblem for each dimension, then the fixed-point iteration is applied. The subproblem for the spatial vector can be regarded as computing a set of reduced-order basis vectors, and the shooting problem projected onto the subspace spanned by these basis vectors is defined to obtain the temporal coefficients. From this procedure, the proposed framework replaces the complex nonlinear time integration of the full-order model with the series of solving simple iterative subproblems. The proposed framework is validated through two descriptive numerical examples considering the conventional linear normal mode method for comparison. The results show that the proposed shooting method based on PGD can accurately capture nonlinear characteristics within 10 modes, whereas linear modes cannot easily approximate these behaviors. In terms of computational efficiency, the proposed method enables CPU time savings of about one order of magnitude compared with the conventional shooting methods.

Keywords Shooting method · Proper generalized decomposition · Steady state response analysis · Nonlinear systems · Reduced order model

1 Introduction

In structural dynamics, the steady-state response of a nonlinear dynamical system plays an important role in understanding the forced vibration characteristics in case of large deformations, nonlinear material behavior, cracks, and boundary conditions with contact. Various attempts have been made to find the steady-state response of a nonlinear dynamical system under periodic excitation, which can be classified into two categories: frequency domain and time domain approaches [1, 2].

The harmonic balance method (HBM) is the frequency domain approach, which relies on the assumption that the steady-state response is represented by a truncated Fourier series [3, 4]. A set of nonlinear algebraic equations for unknown Fourier coefficients is formulated by applying the truncated Fourier series of the solution to the nonlinear differential equation. Since the nonlinear terms are not explicitly defined in the frequency domain, the alternating frequency time (AFT) scheme is usually combined with HBM [5, 6]. Although HBM exhibits fast convergence for weakly nonlinear problems, the response of highly nonlinear problems, e.g., in case of contact cannot be easily captured by the smooth harmonic basis [7].

The shooting method is available for calculating the periodic responses in the time domain. Under general periodic inputs, the steady-state response of a nonlinear dynamic system exhibits periodic characteristics. The shooting method

✉ Yong-Hwa Park
yhpark@kaist.ac.kr

Dae-Guen Lim
ldg0201@kaist.ac.kr

Gil-Yong Lee
lgy@kaeri.re.kr

[1] Department of Mechanical Engineering, KAIST, 291 Daehak-ro Yuseong-gu, Daejeon 34141, Republic of Korea

[2] SMART System Development Division, Korea Atomic Energy Research Institute, 111, Daedeok-daero 989beon-gil, Yuseong-gu, Daejeon 10587, Republic of Korea

Published online: 22 March 2024

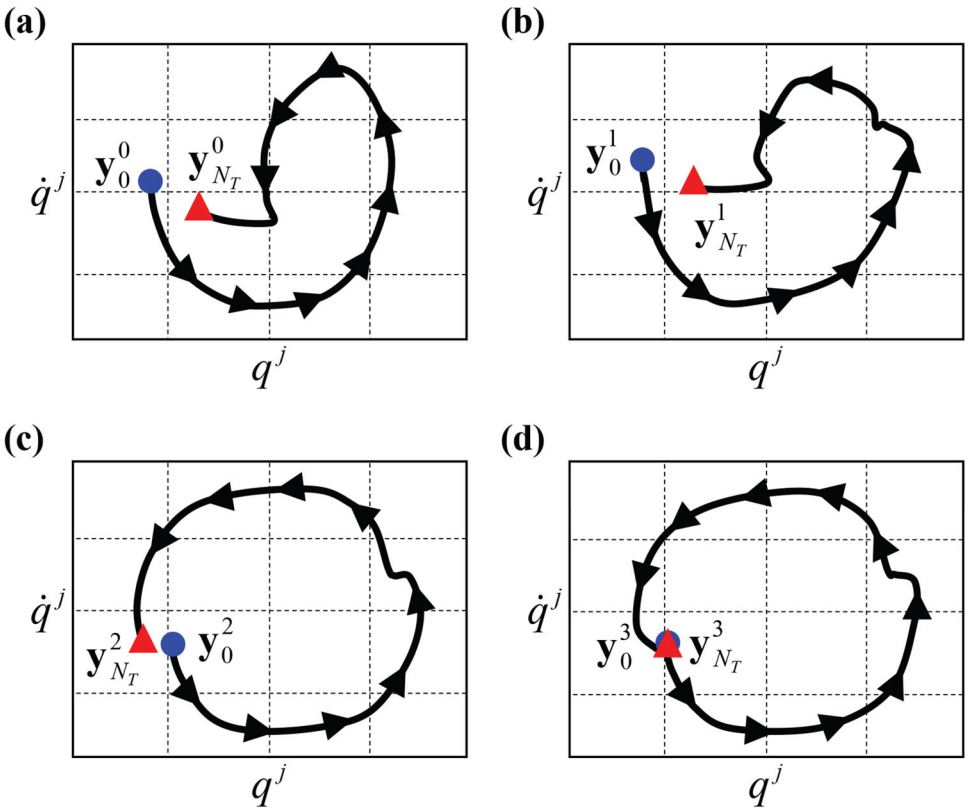

Fig. 1 Iterations of the shooting method: integration of one period **a** from the initial conditions, **b**, **c**, and **d** after the first, second, and final iterations, respectively

formulates a two-point boundary value problem (BVP) to find the initial conditions (i.e. displacement and velocity) of the nonlinear differential equation that satisfy the periodicity condition [8]. The shooting method is advantageous as it easily avoids the cumbersome AFT method and direct time integration for long transient processes, achieving the steady-state response effortlessly by time integrating only the range corresponding to the periodic response. Moreover, the shooting method offers the flexibility to incorporate various types of nonlinearity without assuming that the response characteristics can be accurately represented by approximations such as the Fourier approximation. Recently, various numerical methods have been proposed to analyze vibrations by using the shooting method when non-smooth nonlinear forces such as contact and friction are applied [9, 10]. Studies on the shooting method considering geometric nonlinearities such as large deformations or rotations, have been introduced [11–13].The applications of the shooting method for the analysis of the time response of nonlinear systems, such as stability and optimization, have been reported [14–18]. However, the shooting method still has limitations when solving nonlinear BVP through the Newton–Raphson iteration. The first limitation is that a good initial guess is required for the convergence because the solution is very sensitive to initial conditions. The second limitation is due to computing the derivative of the residual, which makes the algorithm extremely expensive for a large-scale dynamical model [9, 10].

Ensuring computational efficiency in the HBM and shooting method becomes increasingly challenging as the system's degree of freedom expands. Thus, recently with emphasis on computational efficiency, there have been efforts to advance research in model-order reduction (MOR) techniques. As the conventional linear normal mode (LNM)-based MOR technique faces challenges in accurately representing nonlinear system behavior [19], several MOR techniques based on the proper orthogonal decomposition (POD) and proper generalized decomposition (PGD) have been proposed [20–25]. POD has been widely used to compute a reduced-order basis that captures the dominant behavior of a full-order model [23]. The extracted basis is utilized to build a reduced-order model through the Galerkin projection, and the computational efficiency can be accelerated [26]. However, the applicability of POD to the time integration strongly depends on the choice of the time period. This is due to the posterior feature of POD, which applies singular value decomposition to the solution of a full-order model to obtain the reduced-order basis [27]. As an alternative, PGD is a priori model-reduction approach that approximates the solution as a low-rank separated representation [24, 25, 28]. The reduced-order basis associated with the spatial dimension and the corresponding component in temporal dimension are obtained simultaneously [27] without prior knowledge of the response features in contrast to the POD approach [29–31]. Although the price of this advantage is that PGD requires

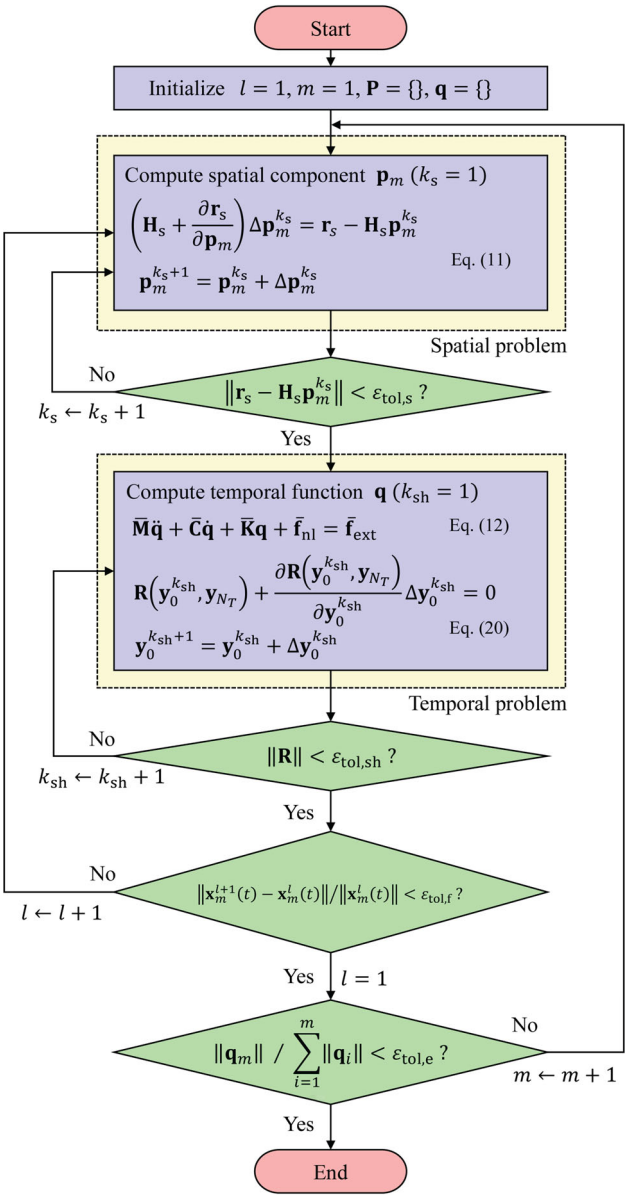

Fig. 2 Flowchart of the proposed framework

additional implementation for formulating subproblems for each dimension, i.e., it effectively alleviates the computational effort through low-rank representation.

This paper presents a novel approach where PGD is combined with a shooting method to tackle the computational inefficiency inherent in the conventional shooting method. The main computational cost of the conventional shooting method arises from the iterative calculation of the inverse of Jacobian matrix using the Newton–Raphson method to obtain the periodic response. As the size of the Jacobian matrix depends on the degrees of freedom (DOFs) of the system, reducing its dimensionality is a crucial aspect in improving computational speed. To reduce the dimension of Jacobian matrix in the shooting method, we employ PGD to separate the periodic response of the equation of motion into spatial and temporal dimensions, followed by formulating subproblems for each dimension, namely spatial and temporal problems, using Galerkin projection. In the temporal problem, the shooting problem is defined by projecting it onto the subspace spanned by the spatial basis vectors. The main concept of the subproblem implementation is equivalent to the various applications of PGD in dynamic problems [31–35]. In the temporal problem, the shooting problem is defined by projecting it onto the subspace spanned by the spatial basis vectors. The initial conditions are non-parametric and represent unknown values that will be determined through Newton–Raphson iteration. Considering that the size of the Jacobian matrix in the temporal problem is determined by the rank of the spatial basis vectors, this approach can yield computational advantages, especially when it is possible to approximate the system with a relatively small number of spatial modes in comparison to its DOFs. To obtain the entire steady-state response, the enrichment is progressively introduced until the PGD approximation satisfies the target tolerance.

The rest of paper is organized as follows. In Sect. 2, the shooting method based on the Newmark integration is described with the Jacobian computation. Section 3 presents the proposed algorithm, which is the use of PGD in the shooting method. In Sect. 4, the performance of the proposed framework is validated through numerical examples. Finally, the conclusions are drawn in Sect. 5.

2 Proper generalized decomposition (PGD) for time-domain analysis of nonlinear system

In this section, we present a model order reduction approach based on proper generalized decomposition (PGD) to address the computational inefficiency associated with time-domain analysis of nonlinear systems. The equations of motion of a nonlinear system with N degrees of freedom (DOFs) under a periodic excitation can be expressed as

$$\mathbf{M}\ddot{\mathbf{x}} + \mathbf{C}\dot{\mathbf{x}} + \mathbf{K}\mathbf{x} + \mathbf{f}_{\text{nl}}(t, \mathbf{x}, \dot{\mathbf{x}}) = \mathbf{f}_{\text{ext}}(t) \tag{1}$$

where $\mathbf{M}, \mathbf{C}, \mathbf{K} \in \mathbb{R}^{N \times N}$ denote the mass, damping, and linear stiffness matrices; $\mathbf{f}_{\text{nl}} \in \mathbb{R}^N$ and $\mathbf{f}_{\text{ext}} \in \mathbb{R}^N$ are the nonlinear force and external force with period T; and, $\mathbf{x}, \dot{\mathbf{x}}, \ddot{\mathbf{x}} \in \mathbb{R}^N$ represent displacement, velocity, and acceleration vectors, respectively. PGD finds the solution of governing equations as a low-rank separated representation, resolving the subproblems defined in each approximation space [24, 25]. In the present context, we approximate the periodic response $\mathbf{x}(t)$ using the spatial vector $\mathbf{p}_i$ and temporal function $q_i(t)$ as follows:

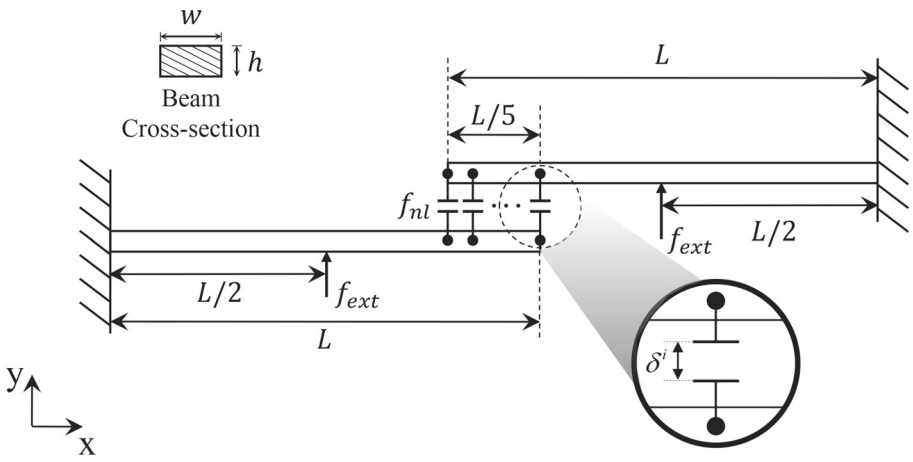

Fig. 3 The nonlinear contact interface between two cantilevers

$$\mathbf{x}(t) \approx \mathbf{x}_m(t) = \sum_{i=1}^{m} \mathbf{p}_i q_i(t) = \mathbf{P}\mathbf{q}(t) \tag{2}$$

where $\mathbf{P}=[\mathbf{p}_1, \ldots, \mathbf{p}_m] \in \mathbb{R}^{N\times m}$, $\mathbf{q}(t)=\{q_1(t), \ldots, q_m(t)\}^{\mathrm{T}} \in \mathbb{R}^m$ and rank m. All components $\mathbf{P}$ and $\mathbf{q}$ with rank m are unknown and should be determined to satisfy the target accuracy. This is a clear difference from other posterior model reduction methods [22, 23] that first construct a basis $\mathbf{P}$ and then compute the expansion coefficients $\mathbf{q}$.

In obtaining the unknown components, we progressively construct the current vector $\mathbf{p}_m$ and update $\mathbf{q}(t)$ through the Galerkin projection, assuming that the previous components $\{\mathbf{p}_i\}_{i=1}^{m-1}$ are already computed. Substituting Eq. (2) into Eq. (1), the nonlinear equations of motions for unknown vector $\mathbf{p}_m$ can be expressed as

$$\mathbf{M}\mathbf{p}_m\ddot{q}_m(t) + \mathbf{C}\mathbf{p}_m\dot{q}_m(t) + \mathbf{K}\mathbf{p}_m q_m(t) + \mathbf{f}_{\mathrm{nl}}(t, \mathbf{P}\mathbf{q}(t), \mathbf{P}\dot{q}(t)) = \mathbf{r}(t) \tag{3}$$

where the residual vector $\mathbf{r}(t) \in \mathbb{R}^N$ is determined by

$$\mathbf{r}(t) = \mathbf{f}_{\mathrm{ext}}(t) - \sum_{i=1}^{m-1}[\mathbf{M}\mathbf{p}_i\ddot{q}_i(t) + \mathbf{C}\mathbf{p}_i\dot{q}_i(t) + \mathbf{K}\mathbf{p}_i q_i(t)] \tag{4}$$

Using a calculus of variations, the test (weight) function for the approximation $\mathbf{x}_m^*(t)$ are obtained by In the calculus of variations, test functions play a crucial role in the derivation of the decomposed subproblems. By considering how the function changes concerning the test function, conditions for minimizing or maximizing a functional are derived.Using a calculus of variations, the test (weight) function for the approximation x_m^* is obtained by

$$\mathbf{x}_m^* = \mathbf{p}_m^* q_m(t) + \mathbf{P}\mathbf{q}^*(t) \tag{5}$$

Multiplying Eqs. (5) to (3), and integrating over the period T, the two equations for each test function $\mathbf{p}_m^*$ and $\mathbf{q}^*(t)$ are formulated as follows:

$$(\mathbf{p}_m^*)^{\mathrm{T}}\left[\left(\int_0^T q_m\ddot{q}_m dt\right)\mathbf{M} + \left(\int_0^T q_m\dot{q}_m dt\right)\mathbf{C} + \left(\int_0^T q_m q_m dt\right)\mathbf{K}\right]\mathbf{p}_m = (\mathbf{p}_m^*)^{\mathrm{T}}\left(\int_0^T q_m(\mathbf{r}-\mathbf{f}_{\mathrm{nl}})dt\right) \tag{6}$$

$$\int_0^T \mathbf{q}^*[(\mathbf{P}^{\mathrm{T}}\mathbf{M}\mathbf{P})\ddot{\mathbf{q}} + (\mathbf{P}^{\mathrm{T}}\mathbf{C}\mathbf{P})\dot{\mathbf{q}} + (\mathbf{P}^{\mathrm{T}}\mathbf{M}\mathbf{P})\mathbf{q} + \mathbf{P}^{\mathrm{T}}\mathbf{f}_{\mathrm{nl}} - \mathbf{P}^{\mathrm{T}}\mathbf{f}_{\mathrm{ext}}dt] = \mathbf{0} \tag{7}$$

Here, Eqs. (6) and (7) are so-called spatial and temporal problems, since each problem is related to the corresponding test function. The Galerkin projection imposes the error, viz., $\mathbf{x}(t) - \mathbf{x}_m(t)$, orthogonal to space spanned by the test function. The proposed framework differs from the conventional Galerkin-based discretization by newly identifying two unknowns $\mathbf{p}_m$ and q_m. Owing to the variation in this approximation, subproblems incorporating presently unknown variables are formulated in a manner distinct from existing methods.

Let us define the operator for Eqs. (6) and (7) by $\mathbf{p}_m = F(\mathbf{q}(t))$ and $\mathbf{q}(t) = f(\mathbf{p}_m)$, respectively [36]. Using these relations, we introduce the following mapping:

$$\mathbf{p}_m = F(\mathbf{q}(t)) \circ f(\mathbf{p}_m) = G(\mathbf{p}_m) \tag{8}$$

Eq. (8) can be seen as a pseudo-eigenproblem, where $\mathbf{p}_m$ can be interpreted as the eigenvector associated with the operator $G(\mathbf{p}_m)$. This interpretation allows the adoption of existing well-known techniques for solving the eigenvalue problem, and fixed-point iteration (power-method) is considered in this work.

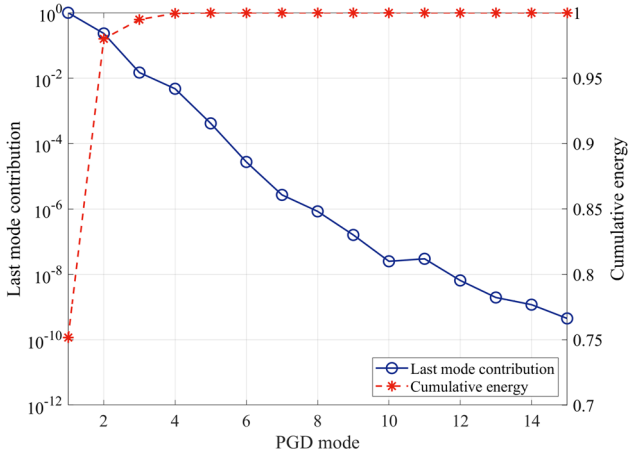

Fig. 4 Evolution of last mode contribution and cumulative energy in the cantilever beam with contact nonlinearity

Assuming that $\mathbf{q}(t)$ is known, the spatial problem (Eq. (6)) is derived as nonlinear equations for $\mathbf{p}_m$ as follows:

$$\mathbf{H}_{\mathrm{s}}\mathbf{p}_m - \mathbf{r}_{\mathrm{s}} = \mathbf{0} \tag{9}$$

where the matrix $\mathbf{H}_{\mathrm{s}} \in \mathbb{R}^{N\times N}$ and residual vector $\mathbf{r}_{\mathrm{s}} \in \mathbb{R}^{N}$ in the spatial problem, which can be obtained by

$$\begin{aligned}\mathbf{H}_{\mathrm{s}} = &\left(\int_0^T q_m\ddot{q}_m dt\right)\mathbf{M} + \left(\int_0^T q_m\dot{q}_m dt\right)\mathbf{C} \\ &+ \left(\int_0^T q_m q_m dt\right)\mathbf{K}\mathbf{r}_{\mathrm{s}} = \int_0^T q_m(\mathbf{r} - \mathbf{f}_{\mathrm{nl}})dt\end{aligned} \tag{10}$$

In order to solve Eq. (10), the Newton–Raphson procedure is applied as follows:

$$(\mathbf{H}_{\mathrm{s}} + \frac{\partial \mathbf{r}_{\mathrm{s}}}{\partial \mathbf{p}_m})\Delta\mathbf{p}_m^{k_{\mathrm{s}}} = \mathbf{r}_{\mathrm{s}} - \mathbf{H}_{\mathrm{s}}\mathbf{p}_m^{k_{\mathrm{s}}} \tag{11}$$

where superscript k_{s} denotes the k_{s}-th iteration count for the Newton–Raphson procedure in the spatial problem. Equation (11) iteratively solved ($\mathbf{p}_m^{k_{\mathrm{s}}+1} = \mathbf{p}_m^{k_{\mathrm{s}}} + \Delta\mathbf{p}_m^{k_{\mathrm{s}}}$) until the criteria $||\mathbf{r}_{\mathrm{s}} - \mathbf{H}_{\mathrm{s}}\mathbf{p}_m^{k_{\mathrm{s}}}|| < \epsilon_{\mathrm{tol,s}}$ is satisfied.

Once Eq. (11) is resolved, a set of spatial functions $\mathbf{P}$ is ortho-normalized by the Gram-Schmidt process to improve the condition of the matrix. The temporal problem (Eq. (7)) then finds the components $\mathbf{q}$, $\dot{\mathbf{q}}$, $\ddot{\mathbf{q}}$ based on the fixed $\mathbf{P}$ and is derived under in period $t \in [0, T]$ as follows:

$$\bar{\mathbf{M}}\ddot{\mathbf{q}} + \bar{\mathbf{C}}\dot{\mathbf{q}} + \bar{\mathbf{K}}\mathbf{q} + \bar{\mathbf{f}}_{\mathrm{nl}} = \bar{\mathbf{f}}_{\mathrm{ext}} \tag{12}$$

where,

$$\begin{aligned}&\bar{\mathbf{M}} = \mathbf{P}^{\mathrm{T}}\mathbf{M}\mathbf{P},\ \bar{\mathbf{C}} = \mathbf{P}^{\mathrm{T}}\mathbf{C}\mathbf{P},\ \bar{\mathbf{K}} = \mathbf{P}^{\mathrm{T}}\mathbf{K}\mathbf{P},\ \bar{\mathbf{f}}_{\mathrm{nl}} = \mathbf{P}^{\mathrm{T}}\mathbf{f}_{\mathrm{nl}}, \\ &\bar{\mathbf{f}}_{\mathrm{ext}} = \mathbf{P}^{\mathrm{T}}\mathbf{f}_{\mathrm{ext}}\end{aligned} \tag{13}$$

Eq. (12) can be seen as the reduced-order model by projecting the Eq. (1) onto the subspace spanned by $\mathbf{P}$, and its reduced dimension is m. The temporal component of this subproblem can be obtained using the usual direct time integration method. Therefore, the rank m is expected to be much smaller than N (i.e., $m \ll N$), and the effort to solve the temporal problem Eq. (12) can greatly improve the computational efficiency of the original problem Eq. (1).

3 Shooting method combined with proper generalized decomposition (PGD)

In this section, we present a novel framework that combines a proper generalized decomposition (PGD)-based model order reduction technique with the shooting method to address computational inefficiency. The primary objective of the shooting method is to determine the initial values. In the temporal problem defined by Eq. (12), the initial values denoted as $\mathbf{y}(0) = \{\mathbf{q}(0)^{\mathrm{T}}, \dot{\mathbf{q}}(0)^{\mathrm{T}}\}^{\mathrm{T}} \in \mathbb{R}^{2m}$ are required to satisfy the following periodicity condition [8]:

$$\mathbf{R} = \mathbf{y}(0) - \mathbf{y}(T) = \{\begin{matrix}\mathbf{q}(0) - \mathbf{q}(T) \\ \dot{\mathbf{q}}(0) - \dot{\mathbf{q}}(T)\end{matrix}\} = \mathbf{0} \tag{14}$$

where $\mathbf{y}(T) = \{\mathbf{q}(T)^{\mathrm{T}}, \dot{\mathbf{q}}(T)^{\mathrm{T}}\}^{\mathrm{T}} \in \mathbb{R}^{2m}$ is the response at the end of the period T. Equation (14) can be seen as a two-point boundary value problem (BVP), where the difference between initial conditions and the responses at $t = T$ is zero.

The numerical implementation of the shooting method consists of two steps: (1) compute $\mathbf{y}(T)$ through the time integration, and (2) adjust the initial condition until $\mathbf{y}(T)$ reaches $\mathbf{y}(0)$ by solving Eq. (14). The graphical illustration of this procedure as the evolution of initial values is presented in Fig. 1. In the first step, time integration can be conducted in either explicit or implicit schemes, and between these two approaches, the implicit Newmark method based on the average acceleration is adopted in this work.

Suppose that the time interval $t \in [0, T]$ is discretized into N_T) time steps with interval. Denoting each time instant by $t_i = i\Delta t (i = 0, \ldots, N_T)$, Eq. (12) at the $i + 1$ step can be written as

$$\begin{aligned}&\bar{\mathbf{M}}\ddot{\mathbf{q}}_{i+1} + \bar{\mathbf{C}}\dot{\mathbf{q}}_{i+1} + \bar{\mathbf{K}}\mathbf{q}_{i+1} + \bar{\mathbf{f}}_{\mathrm{nl}}(t_{i+1}, \mathbf{P}\mathbf{q}_{i+1}, \mathbf{P}\dot{\mathbf{q}}_{i+1}) \\ &\quad = \bar{\mathbf{f}}_{\mathrm{ext}}(t_{i+1})\end{aligned} \tag{15}$$

Based on the average acceleration scheme, the velocity and acceleration vectors at the $i + 1$ step can be approximated by

$$\begin{aligned}\dot{\mathbf{q}}_{i+1} &= \frac{2}{\Delta t}(\mathbf{q}_{i+1} - \mathbf{q}_i) - \dot{\mathbf{q}}_i \\ \ddot{\mathbf{q}}_{i+1} &= \frac{4}{(\Delta t)^2}(\mathbf{q}_{i+1} - \mathbf{q}_i) - \frac{4}{\Delta t}\dot{\mathbf{q}}_i - \ddot{\mathbf{q}}_i\end{aligned} \tag{16}$$

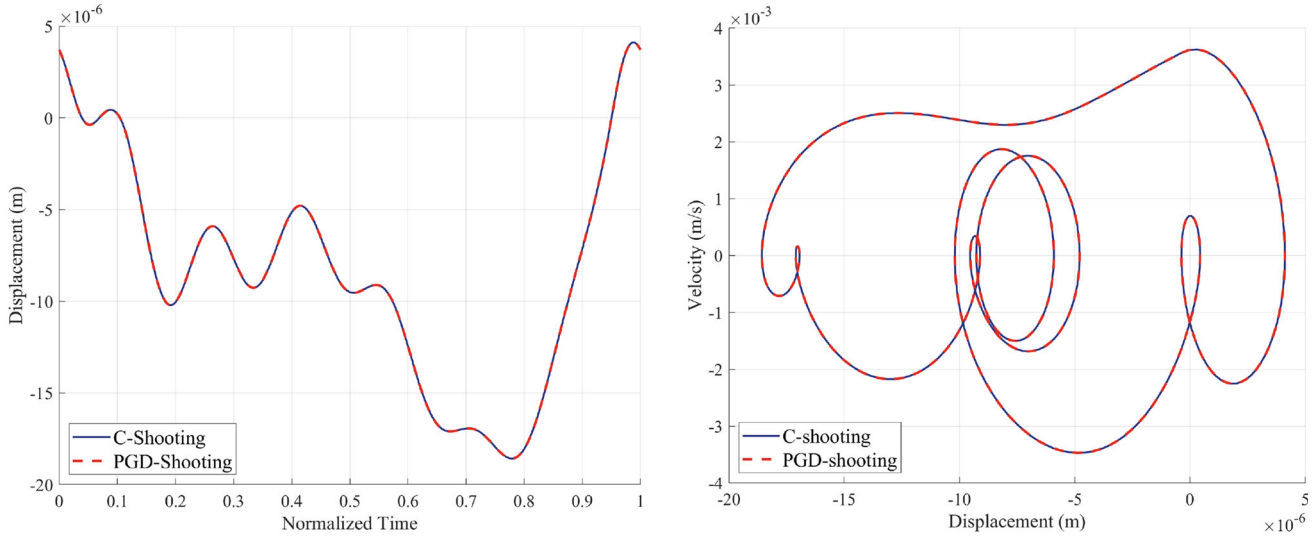

Fig. 5 The time response (left) and phase diagram (right) of the cantilever beam with contact nonlinearity

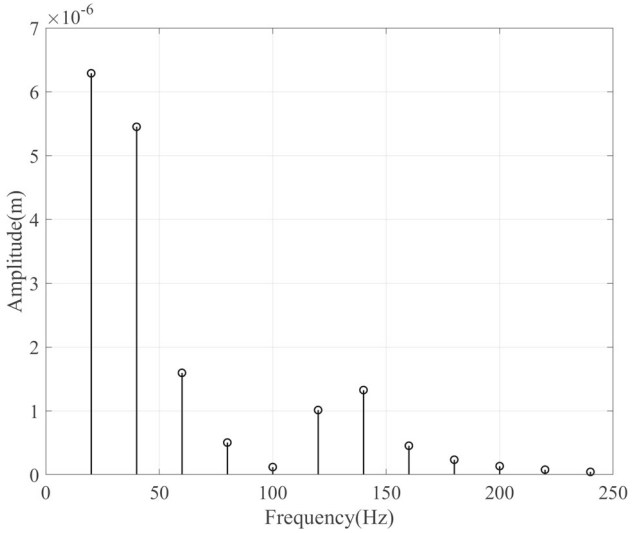

Fig. 6 Spectrum (FFT result) of the time response in the y-direction of the lower beam at the tip node

Substituting Eq. (16) into Eq. (15) yields

$$\mathbf{A}\mathbf{q}_{i+1} = \mathbf{b}(t_{i+1}) - \bar{\mathbf{f}}_{\mathrm{nl}}(t_{i+1}, \mathbf{P}\mathbf{q}_{i+1}, \mathbf{P}\dot{\mathbf{q}}_{i+1}) \tag{17}$$

where the matrix $A \in \mathbb{R}^{m\times m}$ and vector $\mathbf{b} \in \mathbb{R}^m$ in Eq. (17) are computed by

$$\begin{aligned}\mathbf{A} &= \frac{4}{(\Delta t)^2}\bar{\mathbf{M}} + \frac{2}{\Delta t}\bar{\mathbf{C}} + \bar{\mathbf{K}}\\ \mathbf{b}(t_{i+1}) &= \bar{\mathbf{f}}_{\mathrm{ext}}(t_{i+1}) + \bar{\mathbf{M}}\left(\frac{4}{(\Delta t)^2}\mathbf{q}_i + \frac{4}{\Delta t}\dot{\mathbf{q}}_i + \ddot{\mathbf{q}}_i\right)\\ &\quad + \bar{\mathbf{C}}\left(\frac{2}{\Delta t}\mathbf{q}_i + \dot{\mathbf{q}}_i\right)\end{aligned} \tag{18}$$

In order to solve Eq. (17) which is nonlinear, the Newton-Raphson method is applied as follows:

$$\begin{aligned}&\left(\mathbf{A} + \frac{\partial \bar{\mathbf{f}}_{\mathrm{nl}}(t_{i+1}, \mathbf{P}\mathbf{q}_{i+1}^{k_\mathrm{t}}, \mathbf{P}\dot{\mathbf{q}}_{i+1}^{k_\mathrm{t}})}{\partial \mathbf{q}_{i+1}^{k_\mathrm{t}}}\right)\Delta\mathbf{q}_{i+1}^{k_\mathrm{t}}\\ &= \mathbf{b}(t_{i+1}) - \bar{\mathbf{f}}_{\mathrm{nl}}(t_{i+1}, \mathbf{P}\mathbf{q}_{i+1}^{k_\mathrm{t}}, \mathbf{P}\dot{\mathbf{q}}_{i+1}^{k_\mathrm{t}}) - \mathbf{A}\mathbf{q}_{i+1}^{k_\mathrm{t}}\end{aligned} \tag{19}$$

where the superscript k_t denotes the k_t-th iteration count for the Newton–Raphson procedure in the time integration. Under the given tolerance $\epsilon_{\mathrm{tol,NR}}$, Eq. (19) is solved iteratively ($\mathbf{q}_{i+1}^{k_\mathrm{t}+1} = \mathbf{q}_{i+1}^{k_\mathrm{t}} + \Delta\mathbf{q}_{i+1}^{k_\mathrm{t}}$) until the criterion is satisfied as follows:

$$||\mathbf{A}\mathbf{q}_{i+1}^{k_\mathrm{t}} - \left(\mathbf{b}(t_{i+1}) - \bar{\mathbf{f}}_{\mathrm{nl}}(t_{i+1}, \mathbf{P}\mathbf{q}_{i+1}^{k_\mathrm{t}}, \mathbf{P}\dot{\mathbf{q}}_{i+1}^{k_\mathrm{t}})\right)|| < \epsilon_{\mathrm{tol,NR}} \tag{20}$$

Once Eq. (17) is converged to obtain the displacement $\mathbf{q}_{i+1}$, the velocity $\dot{\mathbf{q}}_{i+1}$ and acceleration at the $i+1$ step are easily obtained by Eq. (16).

For the given initial condition $\mathbf{y}_0 = \mathbf{y}(0)$, the solution $\mathbf{y}_{N_T} = \mathbf{y}(T)$ at the time T is obtained by time integration. The next task is to update the initial condition by solving Eq. (14). Until the residual of Eq. (14) meet the criterion $||R|| < \epsilon_{\mathrm{tol,sh}}$, the Newton–Raphson method is again employed by

$$\mathbf{R}(\mathbf{y}_0^{k_\mathrm{sh}}, \mathbf{y}_{N_T}) + \frac{\partial \mathbf{R}(\mathbf{y}_0^{k_\mathrm{sh}}, \mathbf{y}_{N_T})}{\partial \mathbf{y}_0^{k_\mathrm{sh}}}\Delta\mathbf{y}_0^{k_\mathrm{sh}} = 0 \tag{21}$$

where the superscript k_sh is denotes the k_sh-th iteration count for the shooting method ($\mathbf{y}_{i+1}^{k_\mathrm{sh}+1} = \mathbf{y}_{i+1}^{k_\mathrm{sh}} + \Delta\mathbf{y}_{i+1}^{k_\mathrm{sh}}$). The derivative of the residual (i.e., Jacobian) $\partial\mathbf{R}/\partial\mathbf{y}_0 \in \mathbb{R}^{2m\times 2m}$ is computed by

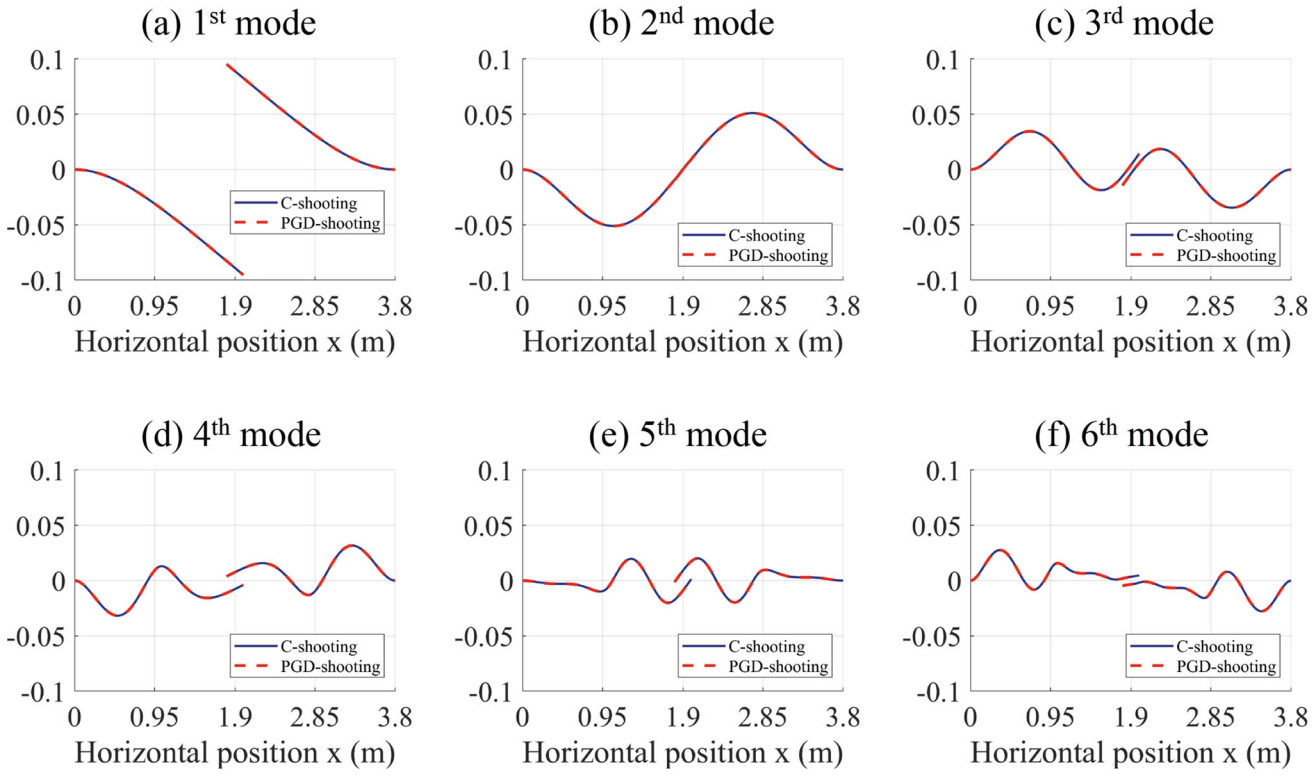

Fig. 7 The first six mode results of C-shooting and PGD-shooting in the cantilever beam with contact nonlinearity

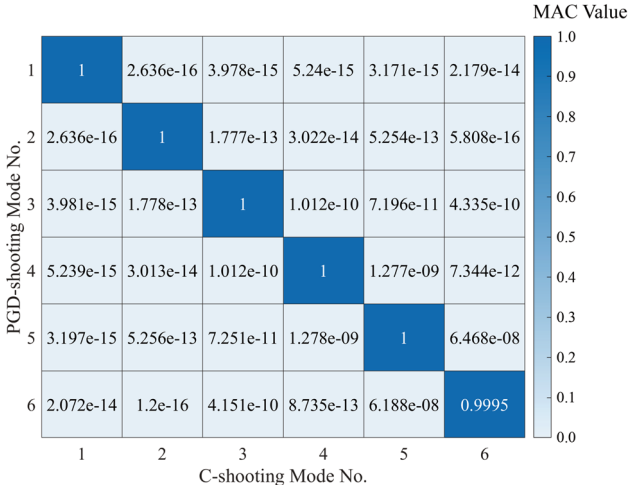

Fig. 8 The modal assurance criterion (MAC) computed by the identified modes obtained from the C-shooting and PGD-shooting methods in the first example

$$\frac{\partial \mathbf{R}}{\partial \mathbf{y}_0} = \frac{\partial (\mathbf{y}_0 - \mathbf{y}_{N_T})}{\partial \mathbf{y}_0} = \mathbf{I} - \begin{bmatrix} \frac{\partial \mathbf{q}_{N_T}}{\partial \mathbf{y}_0} \\ \frac{\partial \dot{\mathbf{q}}_{N_T}}{\partial \mathbf{y}_0} \end{bmatrix} \tag{22}$$

where $\mathbf{I} \in \mathbb{R}^{2m \times 2m}$ is the identity matrix. In order to obtain Eq. (22), taking the derivative of Eq. (17) with respect to $\mathbf{y}_0$ yields

$$\left(\mathbf{A} + \frac{\partial \bar{\mathbf{f}}_{\mathrm{nl}}(t_{i+1}, \mathbf{P}\mathbf{q}_{i+1}, \mathbf{P}\dot{\mathbf{q}}_{i+1})}{\partial \mathbf{q}_{i+1}} \right) \frac{\partial \mathbf{q}_{i+1}}{\partial \mathbf{y}_0} = \frac{\partial \mathbf{b}(t_{i+1})}{\partial \mathbf{y}_0} - \frac{\partial \bar{\mathbf{f}}_{\mathrm{nl}}(t_{i+1}, \mathbf{P}\mathbf{q}_{i+1}, \mathbf{P}\dot{\mathbf{q}}_{i+1})}{\partial \dot{\mathbf{q}}_{i+1}} \frac{\partial \dot{\mathbf{q}}_{i+1}}{\partial \mathbf{y}_0} \tag{23}$$

In the same manner, differentiating Eq. (16) with respect to $\mathbf{y}_0$ yields

$$\begin{aligned} \frac{\partial \dot{\mathbf{q}}_{i+1}}{\partial \mathbf{y}_0} &= \frac{2}{\Delta t} \left(\frac{\partial \mathbf{q}_{i+1}}{\partial \mathbf{y}_0} - \frac{\partial \mathbf{q}_i}{\partial \mathbf{y}_0} \right) - \frac{\partial \dot{\mathbf{q}}_i}{\partial \mathbf{y}_0} \\ \frac{\partial \ddot{\mathbf{q}}_{i+1}}{\partial \mathbf{y}_0} &= \frac{4}{\Delta t^2} \left(\frac{\partial \mathbf{q}_{i+1}}{\partial \mathbf{y}_0} - \frac{\partial \mathbf{q}_i}{\partial \mathbf{y}_0} \right) - \frac{4}{\Delta t} \frac{\partial \dot{\mathbf{q}}_i}{\partial \mathbf{y}_0} - \frac{\partial \ddot{\mathbf{q}}_i}{\partial \mathbf{y}_0} \end{aligned} \tag{24}$$

Inserting Eq. (24) into Eq. (23), the derivative of the displacement vector is obtained as follows:

$$\begin{aligned} \frac{\partial \mathbf{q}_{i+1}}{\partial \mathbf{y}_0} = &\left(\mathbf{A} + \frac{\partial \bar{\mathbf{f}}_{\mathrm{nl}}(t_{i+1}, \mathbf{P}\mathbf{q}_{i+1}, \mathbf{P}\dot{\mathbf{q}}_{i+1})}{\partial \mathbf{q}_{i+1}} \right)^{-1} \\ &\times \left[\frac{\partial \mathbf{b}(t_{i+1})}{\partial \mathbf{y}_0} - \frac{\partial \bar{\mathbf{f}}_{\mathrm{nl}}(t_{i+1}, \mathbf{P}\mathbf{q}_{i+1}, \mathbf{P}\dot{\mathbf{q}}_{i+1})}{\partial \dot{\mathbf{q}}_{i+1}} \right. \\ &\left. \left(\frac{2}{\Delta t} \left(\frac{\partial \mathbf{q}_{i+1}}{\partial \mathbf{y}_0} - \frac{\partial \mathbf{q}_i}{\partial \mathbf{y}_0} \right) - \frac{\partial \dot{\mathbf{q}}_i}{\partial \mathbf{y}_0} \right] \end{aligned} \tag{25}$$

By commencing time integration from the initial time step $t_0 = 0$, the derivative terms $\partial \mathbf{q}_{N_T}/\partial \mathbf{y}_0 \in \mathbb{R}^{2m\times 2m}$ and $\partial \dot{\mathbf{q}}_{N_T}/\partial \mathbf{y}_0 \in \mathbb{R}^{2m\times 2m}$ are finally obtained at the solution of the last step t_{N_T}.

The fixed-point iteration, which solves iteratively the spatial problem and temporal problem, is performed until the following criterion is satisfied from the initial response $\mathbf{x}_m^0(t)$:

$$||\mathbf{x}_m^{l+1}(t) - \mathbf{x}_m^l(t)||/||\mathbf{x}_m^l(t)|| < \epsilon_{\text{tol,f}} \tag{26}$$

where subscript l denotes the l-th iteration count for the fixed-point iteration; $\epsilon_{\text{tol,f}}$ is the tolerance value. After the approximation converges to the fixed values, it is necessary to decide whether to use an additional enrichment step. In this study, the enrichment process is terminated when the contribution of the last mode is less than the tolerance $\epsilon_{\text{tol,e}}$, namely

$$e_{\text{last}} = ||\mathbf{q}_m||/\sum_{i=1}^{m}||\mathbf{q}_i|| < \epsilon_{\text{tol,e}} \tag{27}$$

where e_{last} denotes the last mode contribution. The overall flowchart of the proposed framework is summarized in Fig. 2.

4 Numerical validation

In this section, the proposed framework is validated through three typical but significant engineering examples of nonlinear problems with contact, friction, and crack. In the example problems, Young's modulus $E = 210\,\text{GPa}$, and density $\rho = 7850\,\text{kg}\cdot\text{m}^{-3}$ are assigned to the material properties. The structural damping is considered in the form of proportional damping as follows:

$$\mathbf{C} = \alpha\mathbf{M} + \beta\mathbf{K} \tag{28}$$

where $\alpha = 1$ and $\beta = 10^{-4}$ are the Rayleigh damping coefficients. The external force is limited to periodic excitation, and self-excitation is not considered. The convergence of the proposed method is checked using the last mode contribution e_{last} in Eq. (27) and cumulative energy e_{cum} is defined by

$$e_{\text{cum}} = \sum_{j=1}^{m}||\mathbf{q}_j||/\sum_{i=1}^{M}||\mathbf{q}_i|| \tag{29}$$

where M is the maximum rank. In the time integration of the shooting method, time step $\Delta t = 10^{-4}$ s, the Newton–Raphson tolerance $\epsilon_{\text{tol,NR}} = 10^{-4}$ and the shooting tolerance $\epsilon_{\text{tol,sh}} = 10^{-3}$ are applied. In PGD framework, the fixed-point iteration tolerance $\epsilon_{\text{tol,f}} = 10^{-2}$, and the maximum rank $M = 50$ are used. To compare the accuracy of the proposed approach (PGD-shooting), we consider the method where linear normal modes are applied to the shooting method (LNM-shooting). The conventional shooting method (C-shooting) is considered as the reference [37, 38], and the relative error is computed by:

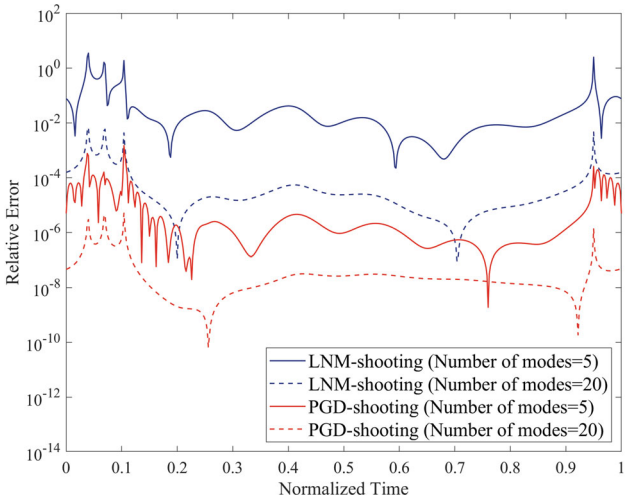

Fig. 9 Relative errors of LNM-shooting and PGD-shooting methods with respect to the number of modes versus time progress in the cantilever beam with contact nonlinearity

$$\epsilon_{\text{rel}} = \frac{||\mathbf{x}_{(\cdot)}(t) - \mathbf{x}_{\text{C-shooting}}(t)||}{||\mathbf{x}_{\text{C-shooting}}(t)||} \tag{30}$$

where $\mathbf{x}_{(\cdot)}$ is either PGD-Shooting or LNM-Shooting methods. Lastly, all the algorithms are developed in MATLAB R2021b and the CPU time was checked for the comparison of computational cost.

4.1 Two cantilever beams with a contact interface

The first example is two cantilever beams with the contact interface, as depicted in Fig. 3. Each beam is modeled as a linear Euler-Bernoulli bending beam with clamped end, discretized by 100 finite elements with 101 nodes. The total DOF of the system is $N = 400$. The length L, width w, and height h are 2 m, 0.3 m, and 0.1 m, respectively. An external force $f_{\text{ext}} = Acos(2\pi ft)$ is applied to the center of each beam. The contact refers to pairs of two nodes situated within the overlapping region of two beams, with a total of 21 contact pairs identified. The penetration depth δ based on two contact nodes is depicted in Fig. 3, and can be defined by

$$\delta^i = u_u^i - u_l^i \tag{31}$$

where the superscript i denotes the index number of a pair of contact nodes; u_u^i and u_l^i are the positions of the upper and

Table 1 Computational efficiency of PGD-shooting compared to the C-Shooting in the cantilever beam with contact nonlinearity. (CPU time of C-Shooting is 132.3 s)

Rank	Contribution of last mode	CPU time (s)	Speed-up
5	4.1397e−04	8.00	16.54
10	2.5208e−08	13.10	10.10
15	4.4996e−10	18.90	7.00
20	3.9774e−11	27.95	4.73

lower part of the cantilever beam at the contact nodes. The contact occurs if $\delta^i < 0$. Based on the penetration depth δ^i, the elastic normal contact force is given by Hunt-Crossley's contact model [39] as follows:

$$f_{nl}^i = \begin{cases} 0 & \text{when } \delta^i \geq 0 \\ k_{\text{cnt}}(\delta^i)^n & \text{when } \delta^i < 0 \end{cases} \tag{32}$$

where k_{cnt} is the contact stiffness, n is the Hertz contact exponent. In this example, the contact parameters $k_{\text{cnt}} = 3.0 \times 10^6$ N/m and $n = 1$ are assigned.

Under the external force $f_{\text{ext}} = Acos(2\pi ft)$ with amplitude $A = 100$ N and excitation frequency $f = 20$ Hz, the last mode contribution along with the cumulative energy of PGD-shooting versus the number of PGD modes is presented in Fig. 4 The obtained results show that as the number of PGD modes increases, the last mode contribution gradually decreases in log-scale and the accumulated energy converges. The number of modes under the target tolerance $\epsilon_{\text{tol,e}} = 10^{-4}$ is six ($m = 6$), which is much less than the DOFs of the given system $N = 400$.

Based on the six PGD modes ($m = 6$), the time response and phase diagram of steady-state response are presented in Fig. 5, and frequency spectrum using fast Fourier transform (FFT) is depicted in Fig. 6. The quantity of interest (QOI) is the y-direction displacement and velocity of the lower beam at the tip node. The time response of the tip displacement is plotted under the normalized time t/T. It can be seen from the results that, due to the contact nonlinearity, the steady-state responses can have multiple frequency components in addition to the excitation frequency $f = 20$ Hz. Although the 1X and 2X frequency components are dominant, the other higher frequency components are not negligible. The proposed framework can accurately estimate this complex nonlinear behavior, implying that PGD can contribute effectively to the shooting method to compute the nonlinear steady-state solutions with fewer modes.

To investigate the dominant subspace of C-shooting, we conduct the singular value decomposition (SVD) onto the response matrix $\mathbf{F} \in \mathbb{R}^{N \times N_T}$ as

$$\mathbf{F} = [\mathbf{x}(0), \cdots, \mathbf{x}(T)] = \mathbf{U}\Sigma\mathbf{V}^{\mathrm{T}} \tag{33}$$

where $\mathbf{U} \in \mathbb{R}^{N \times N}$ and $\mathbf{V} \in \mathbf{R}^{N_T \times N_T}$ denote the unitary matrices. A diagonal matrix $\Sigma \in \mathbb{R}^{N \times N_T}$ is composed of the singular values of $\mathbf{F}$ in the diagonal terms in descending order. The dominant modes are then extracted by selecting the first columns of matrix U. In addition, we considered selecting the diagonal term of matrix Σ to extract eigenvalues and compare the root mean square error of eigenvalues. Six modes are shown in Fig. 7, which indicates the close proximity between the two methods. Also, the root mean square error of eigenvalues $5.8748e^{-10}$. For the purpose of quantitative evaluation, the Modal Assurance Criterion (MAC) matrices are computed as follows [40]:

$$\text{MAC}_{ij} = \frac{|\{\phi_i\}^H\{\phi_j\}|}{\left(\{\phi_i\}^H\{\phi_i\}\right)\left(\{\phi_j\}^H\{\phi_j\}\right)} \tag{34}$$

where i and j are PGD-shooting mode number and C-shooting mode number, respectively. Figure 8 is presented to identify the similarity of modes between two methods. As the diagonal terms of the MAC approach 1, we demonstrate the similarity of the modes obtained from two different methods. This confirms that the proposed PGD can sequentially find the dominant behavior of periodic responses without any precomputation or prior information on response characteristics.

The relative errors (Eq. (29)) of LNM and PGD shooting methods are computed for 5 and 20 modes as shown in Fig. 9. Despite the increment in the relative errors around $0 \leq t/T \leq 0.2$ and $0.9 \leq t/T \leq 1$, PGD-shooing with 5 modes shows that the relative errors are less than 10^{-3} similar to error of LNM-shooting utilizing 20 modes. This indicates that the approximation with PGD-shooting is more accurate than that with LNM-shooting, even with a small number of modes. This is because LNM is obtained by solving the eigenvalue problem of the linearized system, which cannot reflect the contact behavior in the steady-state. However, the proposed PGD-shooting framework by solving spatial and temporal problems catches the most dominant modes, which effectively describe the nonlinear response characteristics.

Finally, the CPU times of PGD-shooting and C-shooting are compared to measure the computational efficiency, as listed in Table 1. The CPU time of PGD-shooting with 5 modes is about 16.54 times faster than that of C-shooting. It is observed that the last mode contribution of the tenth mode is of the order 10^{-8}, which makes it clear that the PGD approximation is converging. In this example, the speed of PGD-shooting is more than 10 times faster than C-shooting. This drastic acceleration in computational efficiency is attributed to the separate representation of the spatial and temporal components in PGD. Especially, since the dimension of the temporal problem in the fixed-point iteration is reduced from $2N$ to $2m$, the computation time can be significantly saved compared to the case of C-shooting.

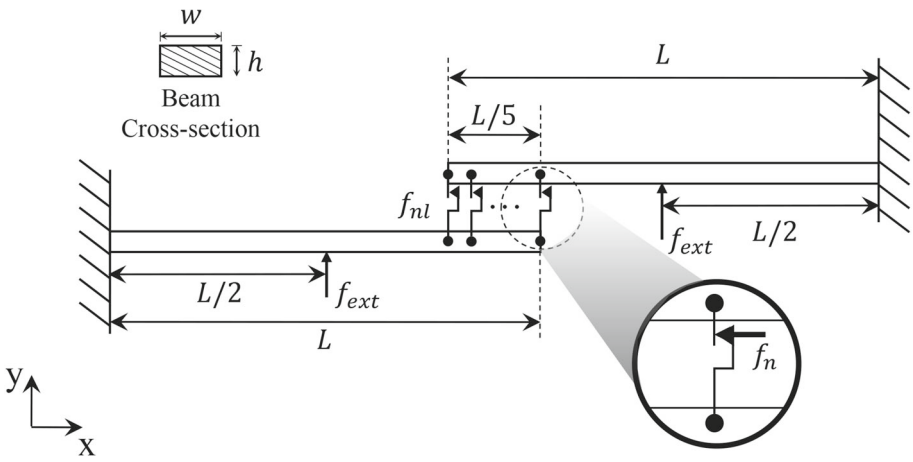

Fig. 10 The nonlinear dry friction interface between two cantilevers

4.2 Two cantilever beams with nonlinear dry friction

The second example replaces the contact pairs in the first example with nonlinear dry friction, as shown in Fig. 10. The friction refers to pairs of two nodes situated within the overlapping region of two beams, with a total of 21 friction pairs identified. The relative velocity based on the two interface nodes can be represented as

$$v^i = v_u^i - v_l^i \tag{35}$$

where the superscript i denotes the index number of a pair of friction nodes; v_u^i and v_l^i are the velocity of the upper and lower part of the cantilever beam at the friction nodes. A pair of friction forces acting on the nodes of each beam is modeled using the smoothed Coulomb friction model as follows [40]:

$$f_{nl}^i = \mu f_n \tanh\left(\frac{v^i}{\epsilon}\right) \tag{36}$$

where μ is the coefficient of friction, f_n is the normal force and ϵ is the conditioning factor, respectively. The dry friction parameters are specified by $\mu f_n = 1\,\mathrm{N}$ and $\epsilon = 10^{-5}$, and external force with amplitude $A = 10\,\mathrm{N}$ and frequency $f = 100\,\mathrm{Hz}$ is applied.

Figure 11 represents the evolution of last mode contribution and cumulative energy of PGD-shooting. The last mode contribution decreases rapidly in the early enrichment steps, and when the tolerance $\epsilon_{\mathrm{tol,e}} = 10^{-4}$ is applied, the PGD-shooting can approximate the response with the seven modes. After sufficient modes are included in which the cumulative energy reaches a converged value, the decaying ratio of the last mode contribution is reduced and can be slightly increased.

Using seven modes under the $\epsilon_{\mathrm{tol,e}} = 10^{-4}$, Fig. 12 represents the time response and phase diagram of steady-state response. The QOI is the y-direction displacement and velocity of the lower beam at the tip node, which is the same as the

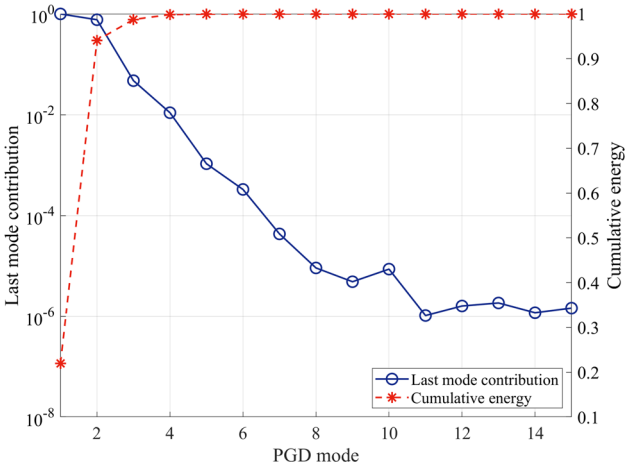

Fig. 11 Evolution of last mode contribution and cumulative energy versus the number of PGD modes in the cantilever beam with dry friction

previous case. The results indicate that the response curves of PGD-shooting and C-shooting are close to each other. Moreover, the phase diagram clearly deviates from the ellipse, indicating that it differs from the perfect ellipse, which is the characteristic of viscous friction in a linear system, due to the nonlinear dry friction.

The dominant modes, which are obtained through SVD from solutions of the C-shooting, are compared with modes from PGD-shooting, and the results are given in Fig. 13. It can be seen that the first five modes exhibit close similarity between two methods, while slight differences are observed in the sixth and seventh modes. Similar to the first example, Fig. 14 illustrates MAC matrices that were used to assess the mutual correlation between modes. The proximity of the diagonal components of the matrix to the value 1 indicates a notable similarity of the modes. The root mean square error of eigenvalues $8.0814e^{-11}$. This similarity confirms that the PGD-shooting mode effectively serves as an approximation for the response of the C-shooting.

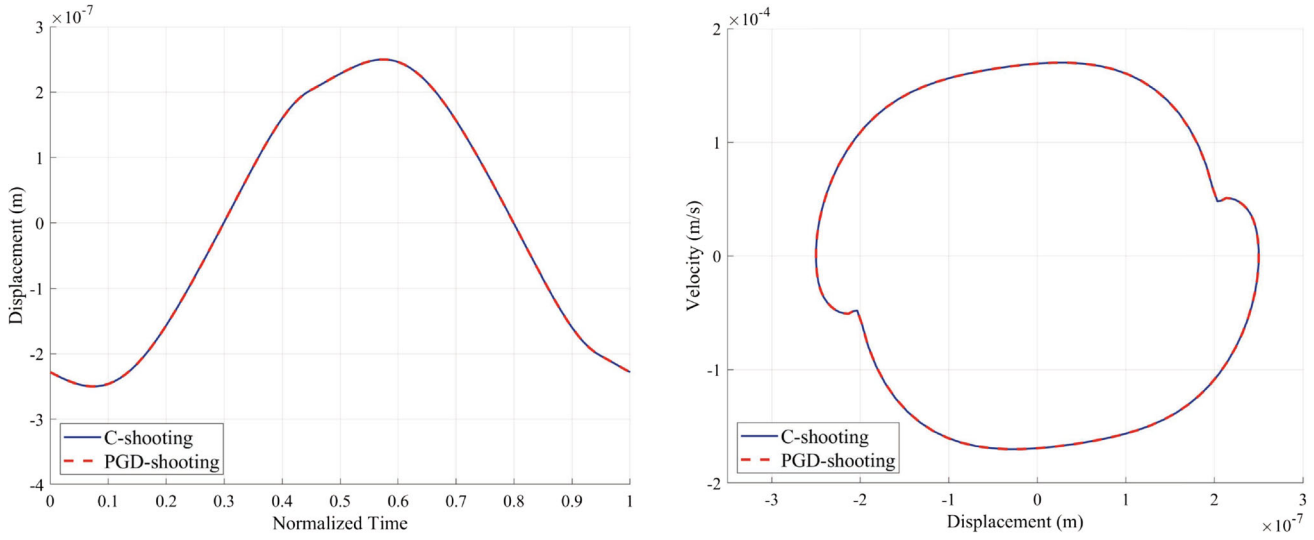

Fig. 12 The time response (left) and phase diagram (right) of the cantilever beam with dry friction

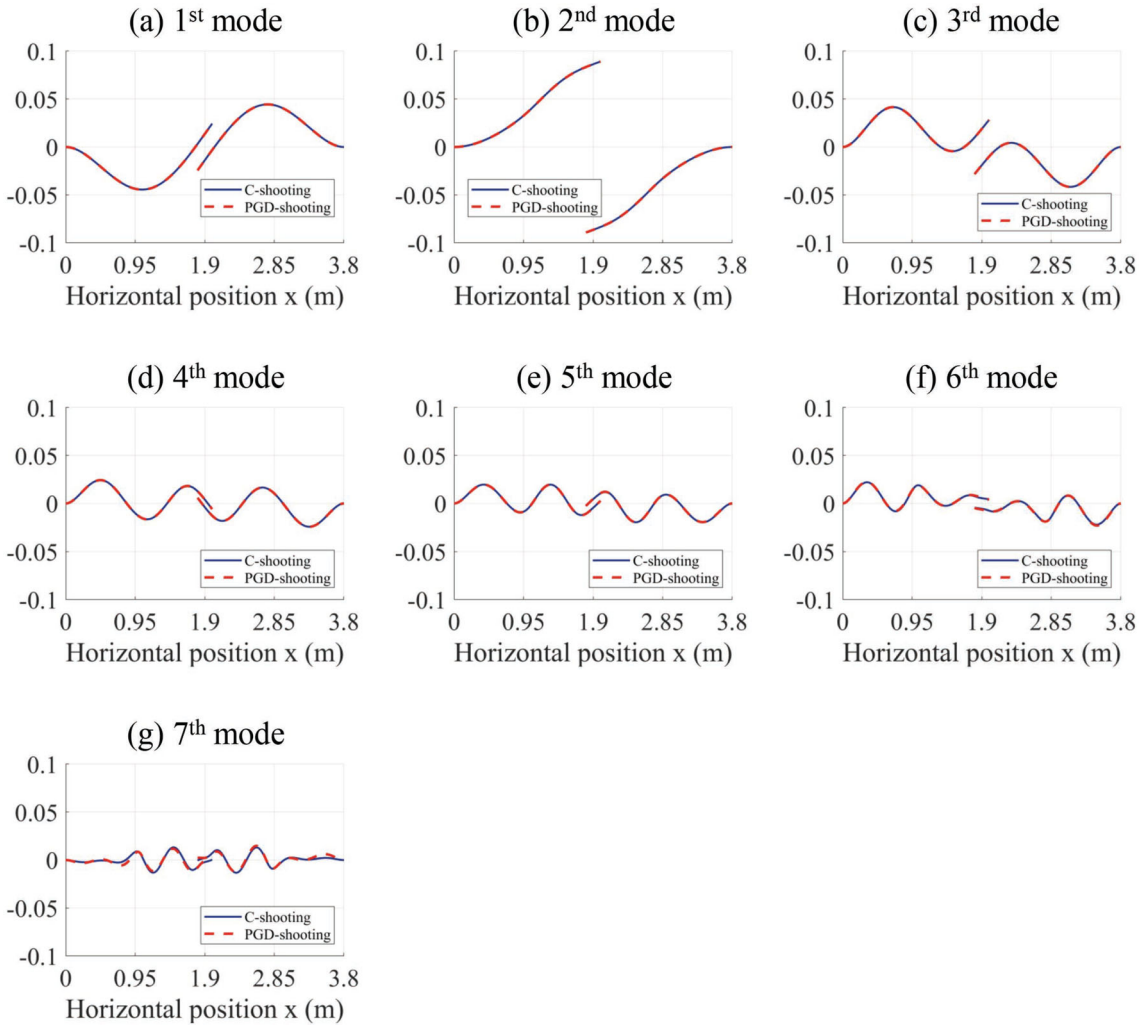

Fig. 13 The first seven modes of C-shooting and PGD-shooting methods in the cantilever beam with dry friction

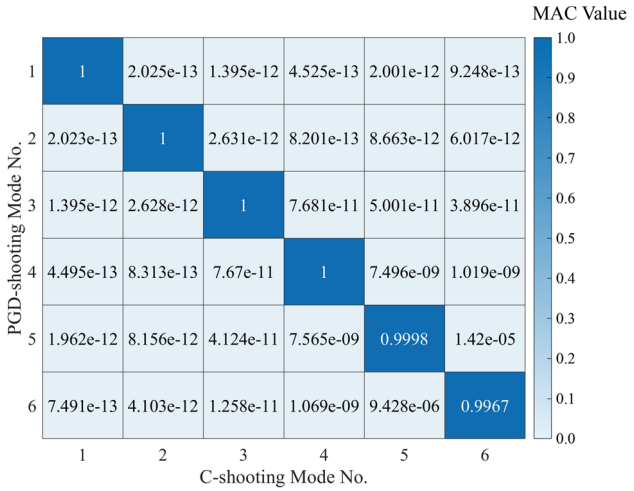

Fig. 14 The modal assurance criterion (MAC) computed by the identified modes obtained from the C-shooting and PGD-shooting methods in the second example

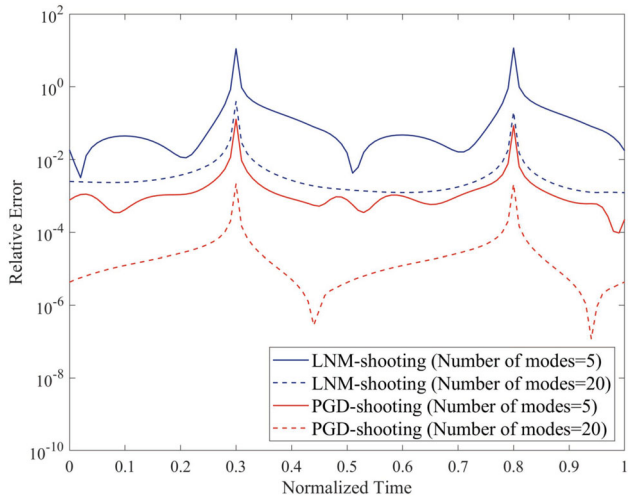

Fig. 15 Relative errors of LNM and PGD-shooting methods for the number of modes in the cantilever beam with dry friction

Figure 15 shows the relative errors of LNM-shooting and PGD-shooting based on the 5 and 20 modes. In this example, there are two points where the response of QOI passes zero, which caused instability in calculating the relative error. Even considering the instability, the relative error of PGD-shooting is smaller than that of LNM-shooting when the same number of modes are applied. Also, the relative error of PGD shooting using 5 modes is smaller than that of 20 linear normal modes. This confirms that LNM is not suitable for accurately approximating the response of the friction nonlinear system in this second example.

The computational efficiency is investigated by varying the rank, and the computational efficiencies are presented in Table 2. The results confirm that PGD-shooting is up to 12.56 times faster than C-shooting. Compared with the previous

Table 2 Computational efficiency of PGD-shooting compared to the C-Shooting in the cantilever beam with contact nonlinearity. (CPU time of C-Shooting is 23.24 s)

Rank	Contribution of last mode	CPU time (s)	Speed-up
5	1.0167e−03	1.85	12.56
10	8.6717e−06	3.71	6.26
15	1.4534e−06	5.12	4.54
20	9.0610e−08	6.84	3.40

contact nonlinearity, it can be seen that the computation time of C-shooting in this example is approximately 6 times faster. This is because dry friction has relatively weak nonlinearity compared to the contact, leading to fast er convergence with fewer iterations. The proposed PGD-shooting also inherited this property, and the CPU time can depend on the type of nonlinearity.

4.3 Cracked structure

The third example is 3D clamped structure with a crack, as shown in Fig. 16. The boundary condition of the example structure is the fixed end at x=0 m. Total 480 hexahedral elements with 873 nodes are used, and total DOF (N) is 2556. The length L, width w, and height h are 2 m, 0.1 m, and 0.3 m, respectively. The crack is located at a distance of 0.2 m away from the fixed boundary surface and has a depth of 0.2 m (2/3 of the height h). An external force $f_{\text{ext}} = Acos(2\pi ft)$ with amplitude $A = 100$ N and excitation frequency $f = 30$ Hz is acting on the right-upper end of the structure.

In this example, a nonlinear contact is caused by the opening and closing phenomenon at the cracked areas. The penetration depth $delta$ is shown in Fig. 16 and can be represented as

$$\delta^i = u_r^i - u_l^i \tag{37}$$

where the superscript i denotes the index number of a pair of contact nodes; u_r^i and u_l^i are the positions of the right and left part of the cantilever beam at the contact nodes. Elastic normal contact force is computed by Eq. (31) when contact occurs if $\delta^i < 0$. The contact parameters $k_{\text{cnt}} = 1.0 \times 10^8$ N/m and the Hertz contact exponent $n = 1$ are applied.

The contribution of last mode and cumulative energy is depicted in Fig. 17 to check the convergence of PGD-shooting. The obtained results show that as the number of PGD modes increases, the last mode contribution decreases and the cumulative energy converges at the early enrichment step. The PGD-shooting can approximate the response with the six modes when the tolerance $\epsilon_{\text{tol,e}} = 10^{-4}$ is applied. Although DOFs in this example are larger than that of the

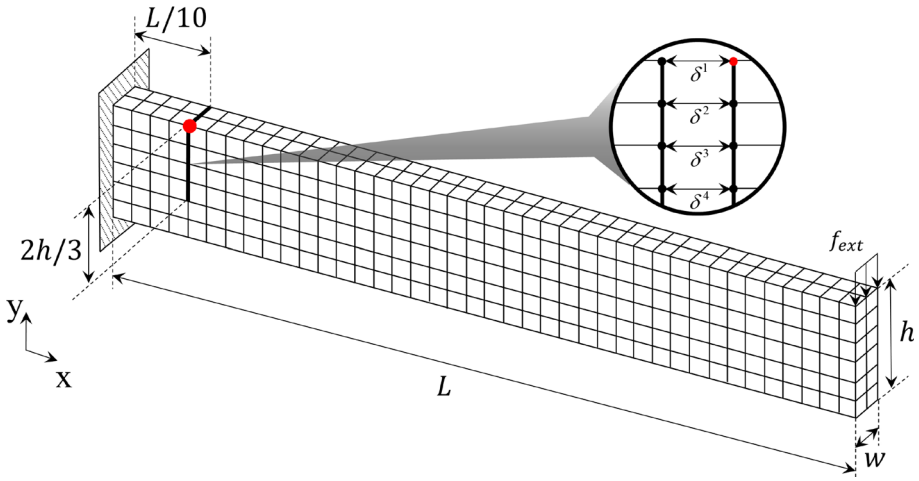

Fig. 16 Cantilever structure with a crack

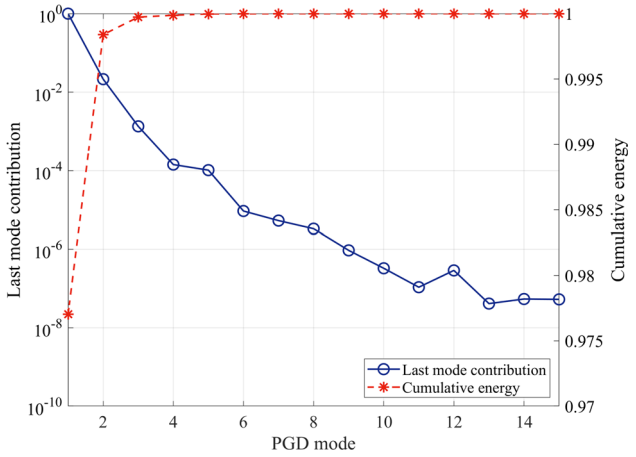

Fig. 17 Evolution of last mode contribution and cumulative energy versus the number of PGD modes in the clamped structure with cracks

first and second cantilevered beam examples, the number of modes to satisfy the target tolerance is less than 10.

Figure 18 represents a comparison of the time response and phase diagram of each method. The x-direction displacement and velocity at the red node in the crack area in Fig. 16 are selected as QOI. Six modes under the tolerance $\epsilon_{\text{tol,e}} = 10^{-4}$ are considered for PGD-shooting, and the LNM-shooting uses the same number of modes obtained from the eigenvalue problem. The nonlinear response obtained from C-shooting and PGD-shooting methods are well-matched to each other. However, LNM-shooting shows a somehow larger difference from both C-shooting and PGD-shooting in Fig. 18, which means that the selected 6 linear normal modes are not suitable for accurately approximating the steady-state solution nonlinear behavior due to crack nonlinearity. In the phase diagram, the crack is closed when a penetration depth is negative, and the crack is opened when they are positive.

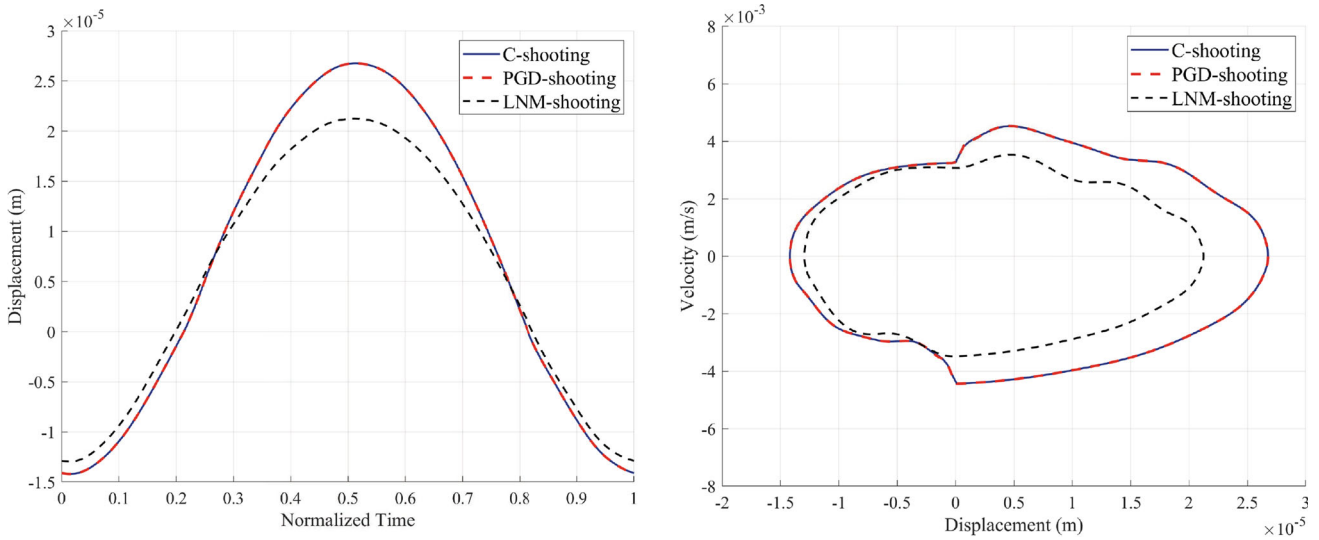

Fig. 18 Comparison of time response (left) and phase diagram (right) in x-direction at a reference point in the cantilever structure with cracks

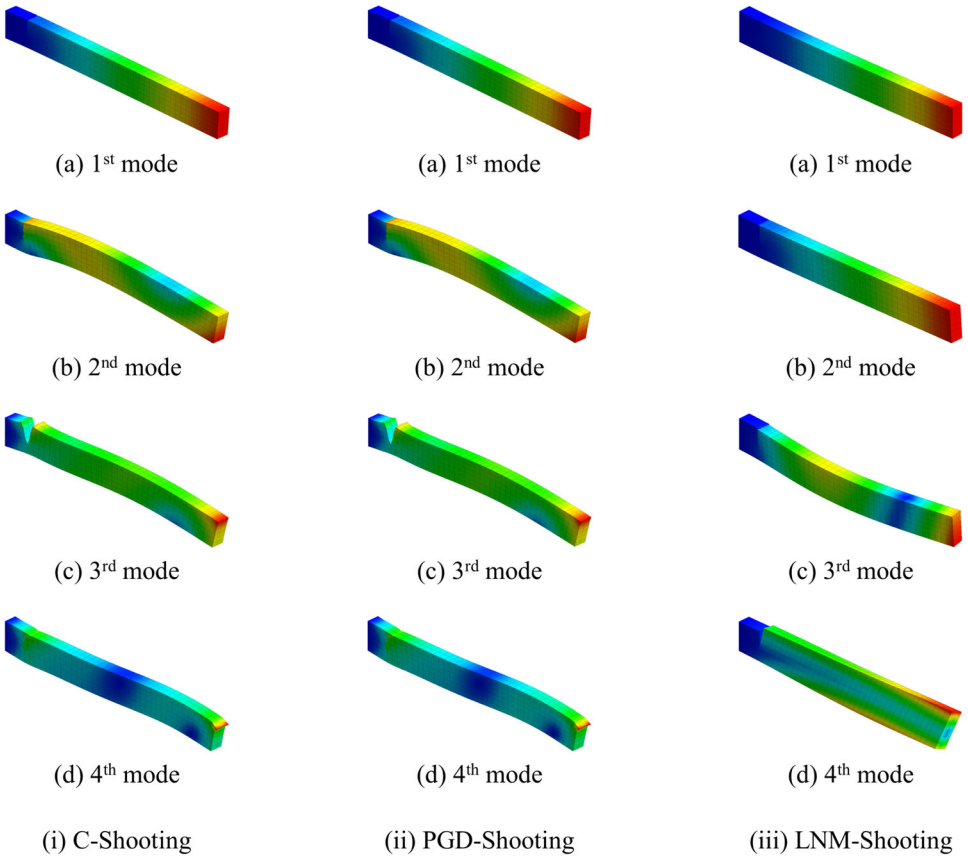

Fig. 19 Comparison of the first four mode shapes between each method(C-shooting, PGD-shooting, LNM-shooting) in the clamped structure with cracks

The LNM-shooting curve does not follow the reference C-shooting solution and PGD-shooting solutions, especially when the crack is opened, viz., right-hand side half of the phase diagram in Fig. 18.

Figure 19 depicts the first four mode shapes used by each method to analyze the reason for the difference in the resulting responses. Moreover, Fig. 20 presents the MAC, which enables an evaluation of the similarity between modes derived from C-shooting method and those obtained through PGD-shooting method. The root mean square error of eigenvalues is $1.3607e^{-9}$. The dominant modes in LNM-Shooting are bending along the y-axis and the torsion, from which it is difficult to approximate the opening and closing phenomena at the crack. However, the PGD-shooting modes sufficiently express the opening and closing nonlinear behaviors, the same as in case of C-shooting modes. This example can effectively show that proposed PGD-shooting can find modal characteristics which correctly capture the local nonlinear characteristics in the vicinity of crack.

Figure 21 shows the relative errors of LNM-shooting and PGD-shooting. The relative error of PGD-shooting using 5 modes is less than 10^{-3}. Also, with 20 modes, the overall relative errors are less than 10^{-4}. However, even though 20 LNMs are used, it is observed that the relative errors of LNM-Shooting hardly dropped below 10^{-2}. This confirms that linear normal modes are insufficient to reflect complex nonlinear behavior. However, the proposed PGD accurately estimates the solution of C-shooting method by sequentially finding the dominant nonlinear behavior due to crack.

Finally, the computational cost is investigated by comparing the CPU times of PGD-shooting and C-shooting, and the results are listed in Table 3. The CPU time of PGD-shooting using 5 modes is about 30.76 times faster than that of C-shooting. The last mode contribution of the 15^{th} mode is approximately of the order 10^{-8}. Even in this case, the speed-up of PGD-shooting is more than about 10 times faster than that of C-shooting. In this example, total DOF ($N = 2556$) is increased about six times compared to the first and second example ($N = 400$). Thus, the dimension of PGD-shooting is reduced from to $m = 6$ under the tolerance $\epsilon_{\text{tol,e}} = 10^{-4}$, which leads to significant acceleration in the computational efficiency compared to C-shooting.

5 Conclusion

In this paper, the PGD-based shooting method is proposed to capture the dominant nonlinear behavior as well as reduce computational efforts compared to the conventional shooting method in calculation of steady-state response of a nonlinear

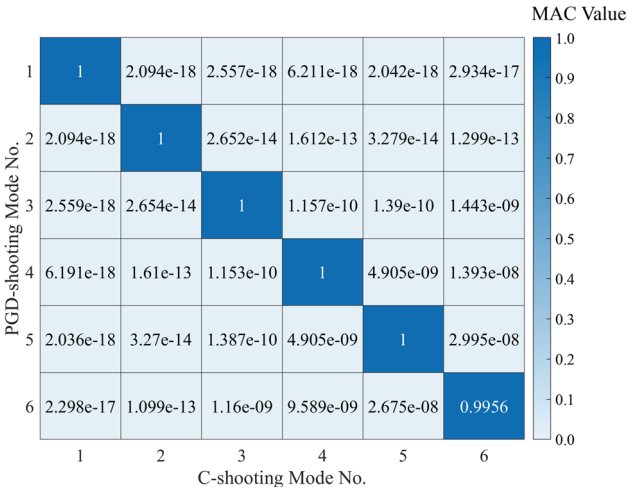

Fig. 20 The modal assurance criterion (MAC) computed by the identified modes obtained from the C-shooting and PGD-shooting methods in the third example

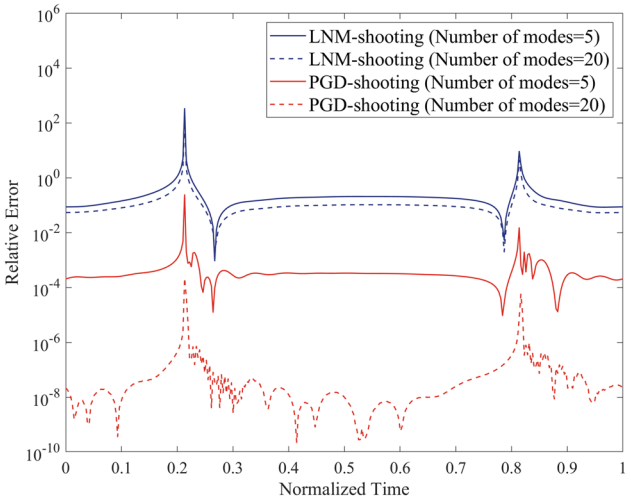

Fig. 21 Relative errors of LNM-shooting and PGD-shooting according to the number of modes: x-direction displacement at the reference point in the cantilever structure with cracks

system. This approach approximates the steady-state solution as a low-rank sum of tensor products of spatial and temporal components. The solution is then sought by successive fixed-point iterations of separated spatial and temporal subproblems, then the enrichment step is applied when the PGD approximation satisfies the target tolerance.

The performance of the proposed method is verified through three examples including cantilever beams with contact and friction interfaces; and a cracked 3D structure. To evaluate the convergence of the proposed framework, we analyzed the contribution of last mode and cumulative energy of modes. In all examples, it is observed that the proposed framework rapidly converges using less than 10 modes. This indicates that nonlinear characteristics can be captured using less than 10 modes, which are very small compared to the total DOF (first and second example: 400, third example: 2556) of the three examples.

Moreover, to assess the accuracy of the PGD approximation, the procedure encompassed the extraction and subsequent comparison of dominant modes. This task was executed through the application of singular value decomposition (SVD) on the response acquired via the utilization of the C-shooting method. Following this step, the computation of the relative error associated with the response was conducted, followed by a comprehensive analysis of the calculated values. The subspace obtained by SVD confirms that PGD can find the dominant behavior without prior computation or knowledge of the nonlinear characteristics, such as contact, friction, and crack. However, linear modes do not correlate well with this nonlinear behavior, and the corresponding relative error decreases slowly as the number of modes increases. Specifically, focusing on the nonlinear behavior of cracks in the third example, when using 20 modes, the error in approximating with linear normal modes is around 10^{-1}, whereas the error drops significantly to 10^{-8} with the PGD modes. This huge difference emphasizes the higher accuracy of the PGD method compared to the linear normal mode method.

Table 3 Computational efficiency of PGD-shooting compared to the C-Shooting in the cantilever beam with contact nonlinearity. (CPU time of C-Shooting is 3441.0 s)

Rank	Contribution of last mode	CPU time (s)	Speed-up
5	1.0257e−04	111.85	30.76
10	3.2401e−07	225.01	15.29
15	5.5042e−08	317.04	10.85
20	1.3050e−08	374.89	9.18

As a result of CPU time comparison to identify the efficiency, the proposed framework, which involves solving separated spatial and temporal problems with rank m below 10, significantly reduced the computational cost compared to C-shooting. The latter deals with the full equation, resulting in total DOF greater than 40 times the rank m. Therefore, although the proposed method requires complex implementation due to decoupled equations, it can be used effectively without any prior knowledge about nonlinearity of the system of interest.

Acknowledgements This research was supported by Korea Electric Power Corporation. (Grant Number: R22XO02-07) This work was supported by the National Research Foundation of Korea (NRF) Grant funded by the Korean government (MSIT). (No. NRF-2020M2D7A107-9180)

Funding Open Access funding enabled and organized by KAIST.

References

1. Krack M, Gross J (2019) Harmonic balance for nonlinear vibration problems, vol 1. Springer International Publishing, Cham, pp 26–28
2. Cochelin B, Vergez C (2009) A high order purely frequency-based harmonic balance formulation for continuation of periodic solutions. J Sound Vib 324(1–2):243–262
3. Lau S, Cheung Y, Wu S-Y (1983) Incremental harmonic balance method with multiple time scales for aperiodic vibration of nonlinear systems. J Appl Mech 50(4a):871–876
4. Pierre C, Ferri A, Dowell E (1985) Multi-harmonic analysis of dry friction damped systems using an incremental harmonic balance method. J Appl Mech 52(4):958–964
5. Cameron TM, Griffin JH (1989) An alternating frequency/time domain method for calculating the steady-state response of nonlinear dynamic systems. J Appl Mech 56(1):149–154
6. Hou L, Chen Y, Fu Y, Chen H, Lu Z, Liu Z (2017) Application of the HB-AFT method to the primary resonance analysis of a dual-rotor system. Nonlinear Dyn 88:2531–2551
7. Gastaldi C, Berruti TM (2017) A method to solve the efficiency-accuracy trade-off of multi-harmonic balance calculation of structures with friction contacts. Int J Non-linear Mech 92:25–40
8. Atkinson K (1991) An introduction to numerical analysis. Wiley
9. Charroyer L, Chiello O, Sinou J-J (2018) Self-excited vibrations of a non-smooth contact dynamical system with planar friction based on the shooting method. Int J Mech Sci 144:90–101
10. Charroyer L, Chiello O (2020) Estimation of self-sustained vibration for a finite element brake model based on the shooting method with a reduced basis approximation of initial conditions. J Sound Vib 468:115050
11. Wang F, Bajaj AK (2007) Nonlinear normal modes in multi-mode models of an inertially coupled elastic structure. Nonlinear Dyn 47:25–47
12. Akhavan H, Ribeiro P (2015) Free geometrically nonlinear oscillations of perfect and imperfect laminates with curved fibres by the shooting method. Nonlinear Dyn 81(1–2):949–965
13. Wang F, Bajaj AK, Kamiya K (2005) Nonlinear normal modes and their bifurcations for an inertially coupled nonlinear conservative system. Nonlinear Dyn 42:233–265
14. Emam SA, Abdalla MM (2015) Subharmonic parametric resonance of simply supported buckled beams. Nonlinear Dyn 79:1443–1456
15. Zhang X, Peng J, Wang L (2014) Parametric resonances in the two-to-one resonant beams on elastic foundation. Nonlinear Dyn 77:339–352
16. Soares RM, Amaral PF, Silva FM, Gonçalves PB (2020) Nonlinear breathing motions and instabilities of a pressure-loaded spherical hyperelastic membrane. Nonlinear Dyn 99:351–372
17. Peng J, Wang L, Zhao Y, Lenci S (2021) Time-delay dynamics of the MR damper-cable system with one-to-one internal resonances. Nonlinear Dyn 105:1343–1356
18. Wang L, Peng J, Zhang X, Qiao W, He K (2021) Nonlinear resonant response of the cable-stayed beam with one-to-one internal resonance in veering and crossover regions. Nonlinear Dyn 103:115–135
19. Kerschen G, Peeters M, Golinval J-C, Vakakis AF (2009) Nonlinear normal modes, part i: A useful framework for the structural dynamicist. Mech Syst Signal Process 23(1):170–194
20. Lu K, Chen Y, Cao Q, Hou L, Jin Y (2017) Bifurcation analysis of reduced rotor model based on nonlinear transient pod method. Int J Non-linear Mech 89:83–92
21. Chinesta F, Ladevèze P (2014) Separated representations and PGD-based model reduction. Fundam Appl Int Centre Mech Sci Courses Lect 554:24
22. Kerschen G, Golinval J-C (2002) Physical interpretation of the proper orthogonal modes using the singular value decomposition. J Sound Vib 249(5):849–865
23. Abbaszadeh M, Dehghan M, Navon IM (2020) A pod reduced-order model based on spectral Galerkin method for solving the space-fractional Gray-Scott model with error estimate. Eng Comput 38:1–24
24. Chinesta F, Ammar A, Cueto E (2010) Recent advances and new challenges in the use of the proper generalized decomposition for solving multidimensional models. Archiv Comput Methods Eng 17(4):327–350
25. Ladevèze P, Passieux J-C, Néron D (2010) The Latin multiscale computational method and the proper generalized decomposition. Comput Methods Appl Mech Eng 199(21–22):1287–1296
26. Georgiou I (2005) Advanced proper orthogonal decomposition tools: using reduced order models to identify normal modes of vibration and slow invariant manifolds in the dynamics of planar nonlinear rods. Nonlinear Dyn 41(1–3):69–110
27. Bamer F, Shirafkan N, Cao X, Oueslati A, Stoffel M, de Saxcé G, Markert B (2021) A Newmark space-time formulation in structural dynamics. Comput Mech 67(5):1331–1348
28. Chinesta F, Ladeveze P, Cueto E (2011) A short review on model order reduction based on proper generalized decomposition. Archiv Comput Methods Eng 18(4):395
29. Chinesta F, Keunings R, Leygue A (2013) The proper generalized decomposition for advanced numerical simulations: a primer. Springer Science & Business Media
30. Cueto E, González D, Alfaro I (2016) Proper generalized decompositions: an introduction to computer implementation with Matlab. Springer
31. Meyrand L, Sarrouy E, Cochelin B, Ricciardi G (2019) Nonlinear normal mode continuation through a proper generalized decomposition approach with modal enrichment. J Sound Vib 443:444–459
32. González D, Cueto E, Chinesta F (2014) Real-time direct integration of reduced solid dynamics equations. Int J Numer Meth Eng 99(9):633–653
33. Lee G-Y, Park Y-H (2021) A proper generalized decomposition based padé approximant for stochastic frequency response analysis. Int J Numer Meth Eng 122(22):6596–6622
34. Lee G-Y, Park K, Park Y-H (2022) Reduced-order modeling via proper generalized decomposition for uncertainty quantification of frequency response functions. Comput Methods Appl Mech Eng 401:115643
35. Lee G-Y, Park Y-H (2023) A proper generalized decomposition-based harmonic balance method with arc-length continuation for nonlinear frequency response analysis. Comput Struct 275:106913
36. Nouy A (2010) A priori model reduction through proper generalized decomposition for solving time-dependent partial differential equations. Comput Methods Appl Mech Eng 199(23–24):1603–1626

37. Rosenberg R (1966) On nonlinear vibrations of systems with many degrees of freedom. Adv Appl Mech 9:155–242
38. Lyapunov AM (1992) The general problem of the stability of motion. Int J Control 55(3):531–534
39. Lugrís U, Escalona J, Dopico D, Cuadrado J (2011) Efficient and accurate simulation of the rope-sheave interaction in weight-lifting machines. Proc Inst Mech Eng Part K J Multi-body Dyn 225(4):331–343
40. Pastor M, Binda M, Harčarik T (2012) Modal assurance criterion. Procedia Eng 48:543–548